Lagrangian Solution for an Irrotational Progressive Water Wave Propagating on a Uniform Current

YANG-YIH CHEN

Department of Marine Environment and Engineering, NSYSU, Kaohsiung, and Department of Hydraulic and Ocean Engineering, NCKU, Tainan, Taiwan

HSUAN-SHAN CHEN, CHU-YU LIN, AND MENG-SYUE LI

Department of Marine Environment and Engineering, NSYSU, Kaohsiung, Taiwan

(Manuscript received 13 August 2012, in final form 2 November 2012)

ABSTRACT

Experiments are conducted to measure the motion properties of water particle for the progressive water wave propagation in the presence of following and adverse uniform currents. The experimental data are used to validate the fifth-order Lagrangian solution from Chen and Chen. The experimental results show that the measured data of the particle motion properties such as the *b* line (denoted as the line connecting the positions of consecutive particles of the same *b* label), the particle velocity, the particle transport velocity (drift velocity), the particle trajectory, the particle motion period, and the Lagrangian mean level are in close agreement with those of the fifth-order Lagrangian solution. The study also shows that the particle label could adopt the position coordinates of the particle as if it were in still water. The motion of the *b* line oscillates like wave motion: its wavelength is equal to the progressive wavelength and its wave velocity obeys the Doppler effect so the sum of the velocities of the progressive wave and current, the particle motion period, the Lagrangian mean level, and the particle transport velocity less current velocity are the same as for the case of pure progressive waves.

For following currents, the shape of particle trajectory depends on the horizontal particle velocity at the trajectory trough. For adverse currents, the shape of particle trajectory depends on the horizontal particle velocity at the trajectory crest.

For a description of the flow motion, the Lagrangian solution could be more effective and precise than the Eulerian solution.

1. Introduction

Previous studies on the wave–current interaction have usually adopted the Eulerian approach to describe particle motions at fixed spatial positions in the wave–current field, such as Longuet-Higgins and Stewart (1960, 1961), Jonsson et al. (1970, 1978), Jonsson (1977), Peregrine (1976), Thomas (1981, 1990), Baddour and Song (1990), Groeneweg and Battjes (2003), Musumeci et al. (2006), Olabarrieta et al. (2010), etc. However, the results obtained by the Eulerian approach are hard to precisely depict motion properties of water particles such as the particle trajectory, the particle motion period, drift velocity, the Lagrangian mean level, and streaklines. More effectively and precisely, Lagrangian approach is employed for analysis and measurement of the particle motion in the wave–current field. Chen et al. (2012) have solved the wave–current interaction up to the third order in the Lagrangian approach. The particle displacement, the Lagrangian wave frequency, the Lagrangian mean level of particle motion, and mass transport can be obtained directly from the third-order Lagrangian solution. For the comparison of the particle motion properties to the higher waves, the third-order solution does not fit well as expected with the experiment data, however.

For Lagrangian measurement, the motion of water particles is generally affected by the size and density of a trace particle, and its trajectory is different between the photographed and actual positions. Only a few studies have implemented a Lagrangian measurement for particle motions in a flow field; for these studies only

Corresponding author address: Yang-Yih Chen, Dept. of Marine Environment and Engineering, NSYSU, No. 70, Lienhai Rd., Kaohsiung 80424, Taiwan.
E-mail: yichen@mail.nsysu.edu.tw

DOI: 10.1175/JTECH-D-12-00171.1

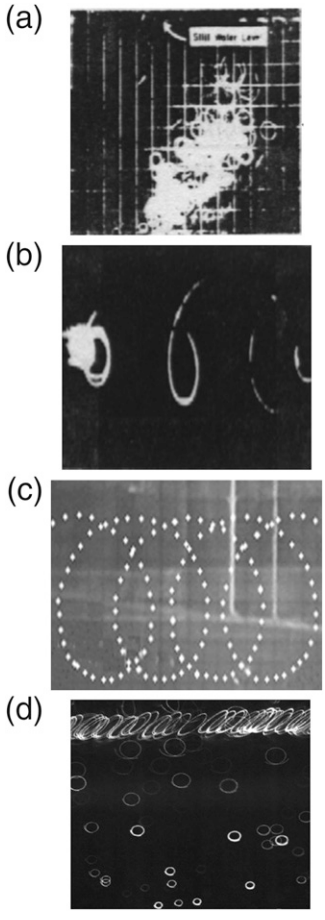

FIG. 1. (a) Photo of trajectories of fluorescent particles by Morison and Crooke (1953). (b) Photo of streaklines of fluorescent particles by Longuet-Higgins (1986). (c) Photo of trajectory of PS particles by Chen et al. (1998). (d) Photo of small particle trajectories using PIV by Pullen et al. (1998).

qualitative results are reported. For the free-surface periodic progressive wave field, Fig. 1a shows the trajectory of the fluorescent particles photographed by Morison and Crooke (1953); Fig. 1b shows the streaklines of the fluorescent particles photographed by Longuet-Higgins (1986); and Fig. 1c shows the trajectory of the polystyrene (PS) photographed by Chen et al. (1998). The PS particle is 1 mm in diameter with the density close to water. For the capillary–gravity wave field, Fig. 1d shows the trajectory photographed by Pullen et al. (1998) using particle imaging velocimetry (PIV).

There are two main reasons for not being able to directly and precisely quantify Lagrangian measurements: one is the size and density of the trace particle, which could be overcome easily, using the thermal-treated, industrial fluorescent polystyrene particles in this study, and the other is that when photos are taken under the same shooting condition, the image position deviation occurs if the gridded coordinate plane and the plane of the particle motion are not coplanar. To clearly understand the phenomenon of the image position deviation, considering two identical gridded planes, one marked with an x at each grid point and another with marked with an ○ when these two planes are not coplanar; photos are taken to create the image deviation as shown in Fig. 2a. Figure 2b shows no deviation when the two planes are coplanar. Based on this kind of deviation, a procedure for geometrical adjustment to correctly quantify the measured data could be easily worked out. This procedure has been used by Chen et al. (2010) for positioning particle trajectory in the wave field. In this study, the same procedure is further applied to the wave–current field. The current could be in the following or adverse direction. Measured data of particle motion properties are used for validation of the fifth-order Lagrangian solution given in Chen and Chen (2013, manuscript submitted to *Commun. Math. Phys.*)

Section 2 describes the apparatus and setup of the experiments. Section 3 describes the conditions and protocol for the experiment, and the comparisons of the motion properties of particles between the measured data and the fifth-order Lagrangian solution. Section 4 describes the major properties of particle motions that are validated by the measured data. Finally, section 5 provides the conclusions for this study.

2. Experimental setup and procedure

This experiment is to investigate motion properties of the particles for the progressive waves in the presence of uniform current in water of constant depth. The current could be in the following or adverse direction. The experimental setup, procedure, and apparatus are described as follows.

a. Experimental setup

This experiment is conducted in a glass-walled wave–current flume at the Department of Marine Environment and Engineering, National Sun Yat-Sen University (NSYSU). The flume is 35.0 × 1.0 × 1.2 m (length, width, height, respectively) and is capable of generating the following and adverse circulating currents. Five parallel metal vanes (63.5, 127, 190.5, 127, and 63.5 cm long, 26 cm high, and 0.3 cm thick; 17 cm apart for each) are installed at the two ends of the flume bed for generating uniform currents. A high-speed camera is set up in front of the observation window at about 15 m away from the wavemaker for continuously photographing the motion of the trace particles. To avoid interfering with the particle motion on the (vertical) x–y plane, the four wave gauges are placed at 9, 14, 16, and

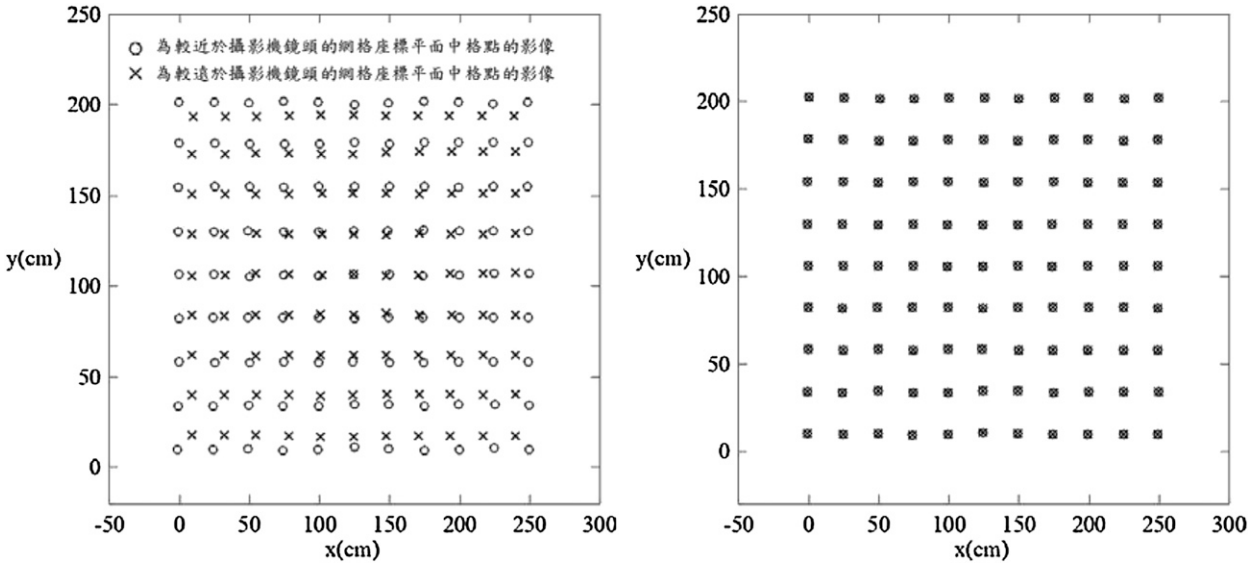

FIG. 2. Gridpoint images of two same gridded planes marked with × (far plane from camera) and ○ (near plane) respectively: (a) position deviation when two planes are not coplanar and (b) no position deviation when two planes are coplanar.

22 m, respectively, away from the wavemaker and 10 cm off the middle width of the flume (see Fig. 3b) to measure the incident waves. Three current meters are placed at about 12.6 m away from the wavemaker at 35, 45, and 65 cm, respectively, away from the glass wall, and 48.2, 20.4, and 6.0 cm, respectively, below the surface of the still water to measure the flow velocity of the following and adverse currents. For measurement of particle trajectories, a copper rod (1.5-m length, 5-mm diameter with 3-mm-diameter round holes 5 cm apart) is placed vertically at the middle width of the flume. The PS particles are released through the opening and closing of the round holes. Prior to measurement we need to observe the net drift of the released PS particle to decide the release position, which must be placed upstream from the net drift; this is to make sure the PS motions are in the area that could be photographed through the observation window. We further require that at least five consecutive similar waves be recorded by wave gauge 2 and 3 as the PS particle moves through the observation area. At the end of the flume about 8 m long, a rubberized fiber beach with 1:10 slope, as described by Davies and Heathershaw (1984), was built to prevent wave reflection. Note that twice the beach length accommodates more than four of the longest wavelengths in the experiment, and it is expected to absorb shorter waves even more effectively. The experimental setup is schematically shown in Figs. 3a–c.

b. Measurement apparatus and procedure

1) Wavemaker: A computer-program-driven, electrohydraulic, piston-type wavemaker is used to generate monochromatic waves. The period of generated wave could be adjusted by 0.01-s increments. The shortest period is 0.08 s. Its accuracy could be calibrated to be in the error range of 0.1–0.3 s for every 60 consecutive waves; the accuracy of the generated wave period is within ±0.005 s.
2) Wave gauge and current meter: A MK5-3X-L100-D3 capacity wave gauge and an ACM200-A electromagnetic current meter made in Japan are used for measurement of water elevation and current. Both apparatus have linear output property.
3) Tracer particle: Industrial fluorescent PS particles of 1-mm diameter are used as the tracer particle. Its original density is about 1.05 g cm^{-3}, slightly heavier than water. After the PS particles are boiled in water, expanded, and cooled off, their density became nearly equal to water density, 1.000 g cm^{-3}, which is able to keep the PS particle at a stable fixed position in the still water.
4) High-speed camera: An A301fc-type high-speed camera from Basler Company capable of photographing 80 frames per second (fps) is used to photograph the particle motion. Its BCamGraber program is used to control the camera for collecting the image data, which are then processed and analyzed using MATLAB software.
5) Four 110-V–500-W lamps: Four powerful lamps are set up to enhance brightness for easy identification of the PS motion images.
6) A gridded plate: Limited by the length of the observation window, which is 1.0 m, a transparent acrylic-plastic plate (80 long × 45 high × 0.2 cm

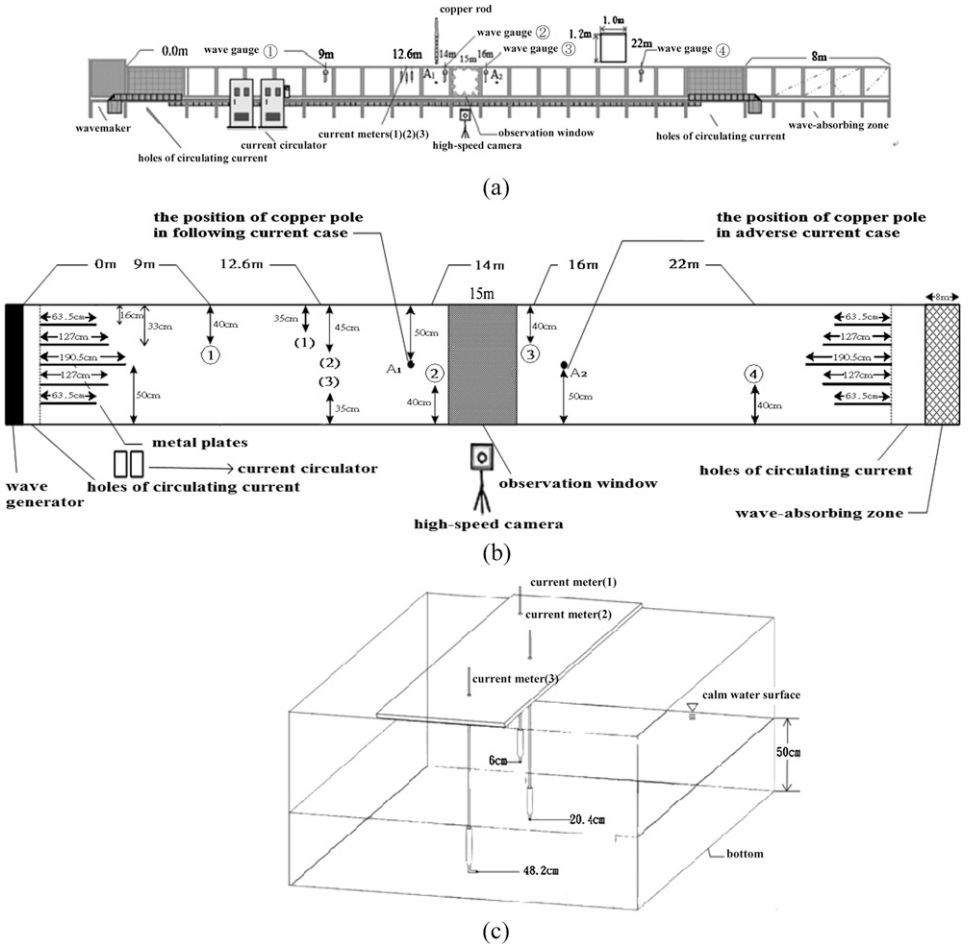

FIG. 3. Schematic of the experimental layout. (a) Front view of the flume cross section. (b) Top view of the flume cross section. (c) Positions of the three current meters (numbers with circles: wave gauge positions; numbers with parentheses: current meter positions).

thick) is used to make a gridded plate. The plate is marked horizontally and vertically with 0.5-cm dash lines to make a grid network of 30 × 16 squares with each square 2.5 × 2.5 cm. This gridded plate is placed at the middle width of the flume in the vertical position, facing the observation window, in the still water. Then it is photographed before being removed from the flume. The grid network in the photo is digitalized and used as the reference for positioning and analyzing the consecutive images of the PS particles photographed by the high-speed camera.

7) A copper rod and PS release: A copper rod (1.5-m length and 0.5-cm diameter) has carved marks every 0.1 cm. It is perforated below 70 cm with holes of 0.3-cm diameter at 5-cm intervals. The holes are opened or closed using the valves. To continuously photograph the PS moving through the observation window, the PS must be released at an upstream position (refers to direction of the net PS transport); specifically, when the net PS transport is toward the beach end of the flume, the rod must be placed at position A_1 shown in Figs. 3a and 3b for the PS release; likewise, when the net PS transport is toward the wavemaker end, the rod must be placed at position A_2.

Now with the rod at the proper position, the current is then generated to reach a stably, uniformly designated speed that is monitored by the three current meters as shown in Fig. 4a. At this time the valve on the rod is opened to release a PS particle, and in the meantime a train of the designated progressive waves is generated. The released PS particle moves cyclically through the observation window, and during this period of time it is photographed by the high-speed camera. Criteria are

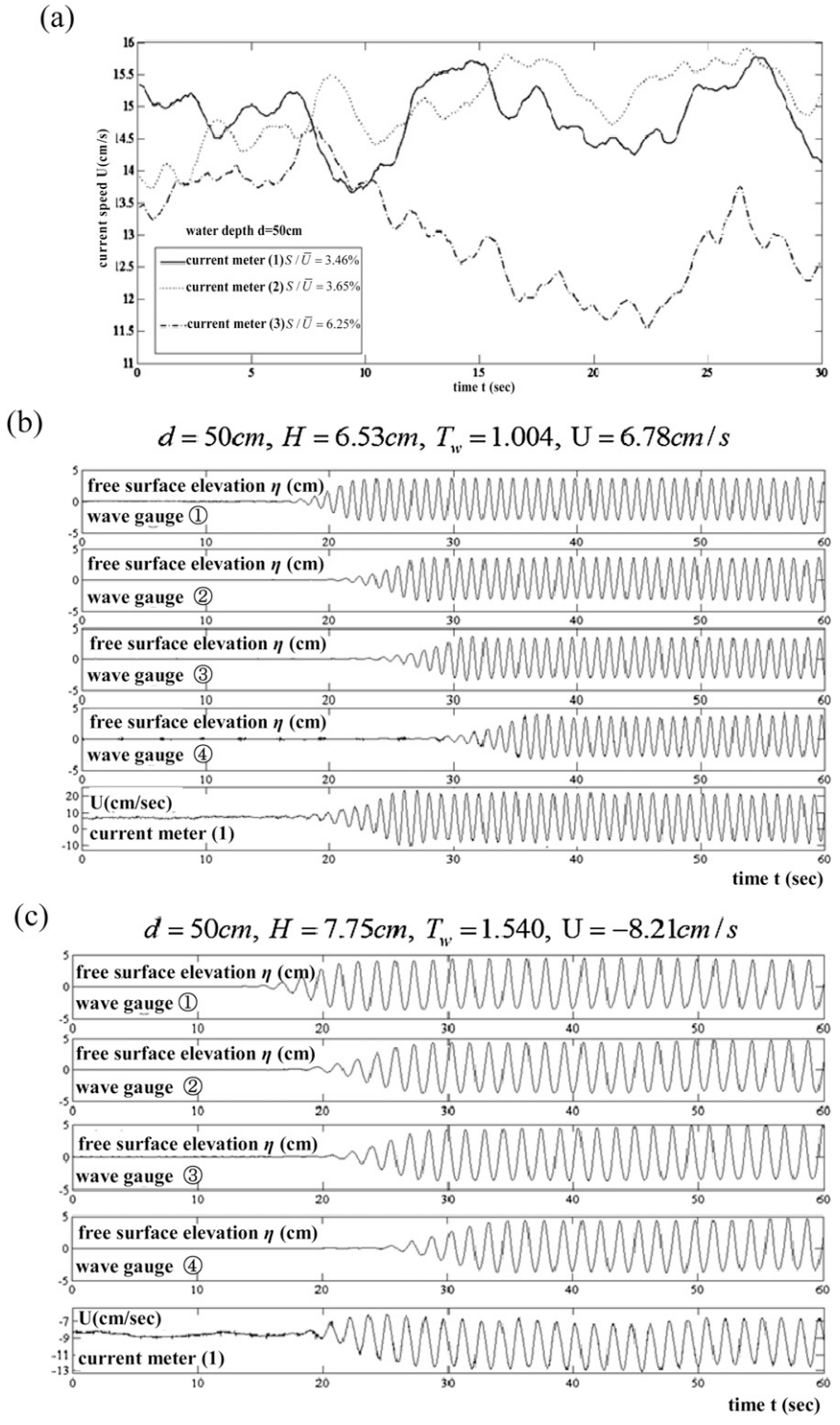

FIG. 4. (a) Typical currents at three current meters (1), (2), and (3); S is standard deviation and $\overline{U}$ is mean current speed. (b) Typical waves at wave gauges with a following current. (c) Typical waves at wave gauges with adverse currents. Note that after a short time from the start, the waves are periodic steady state with similar individual waves.

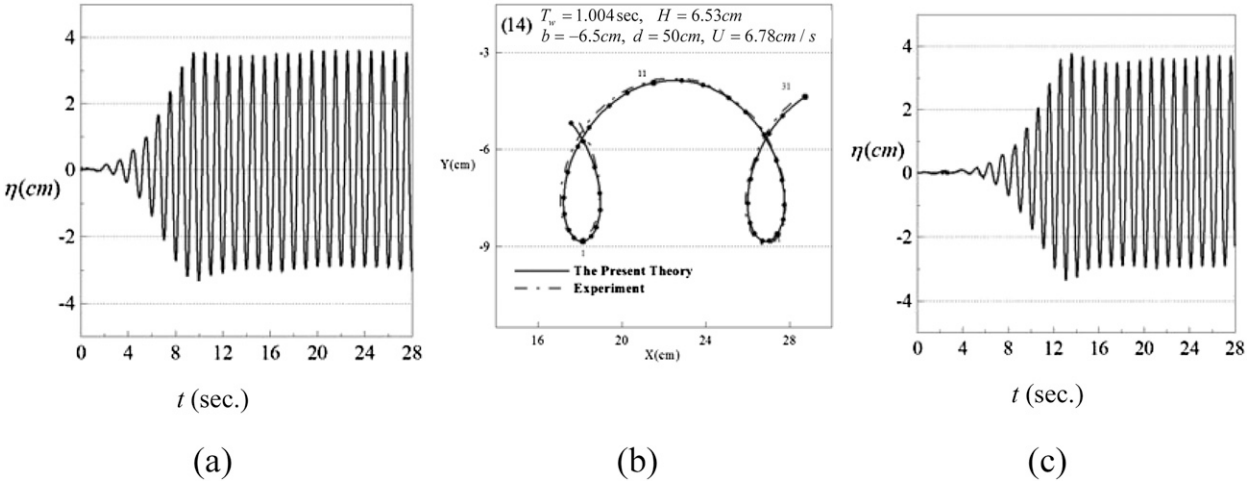

FIG. 5. Progressive wave with a following current: (a) waves at wave gauge 2, (b) measured and PS-theory trajectory, and (c) waves at wave gauge 3. Note that after a short time from the start, the waves are periodic steady state with similar individual waves.

also set that, during this same period of time, the waves at wave gauges 2 and 3 at the upstream and downstream positions, respectively, of the observation window are required to record at least five consecutive similar waves as shown in Figs. 4b and 4c.

For the case of no current, the experimental procedure is the same as in Chen et al. (2010). The rod is placed at the middle width of the flume and inside the area of the observation window. A PS particle is released into the still water and then the rod is slowly removed out of the water. Then the wavemaker is started and the particle motion is photographed.

The experiments are conducted for three different types of current: the following current, no current, and the adverse current. The observation results are shown in Figs. 5–7.

3. Experimental results

In the experiments, the still water depth d is set mostly 50 cm to avoid a deeper water depth, which may cause difficulty in generating uniform currents. The generated currents are measured at the three current meters, which are placed at three different depths with one current meter near the bottom. The generated wave in the presence of the current is measured at the four wave gauges. Results of the currents and waves at the four gauges are shown in Fig. 4. Figure 4a shows that after

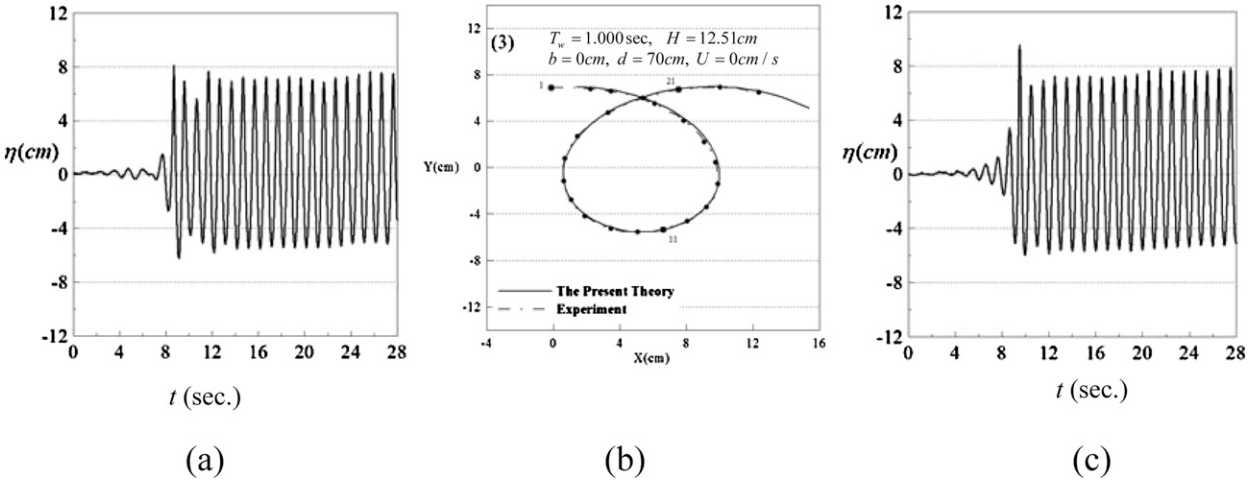

FIG. 6. As in Fig. 5, but for progressive waves with no current.

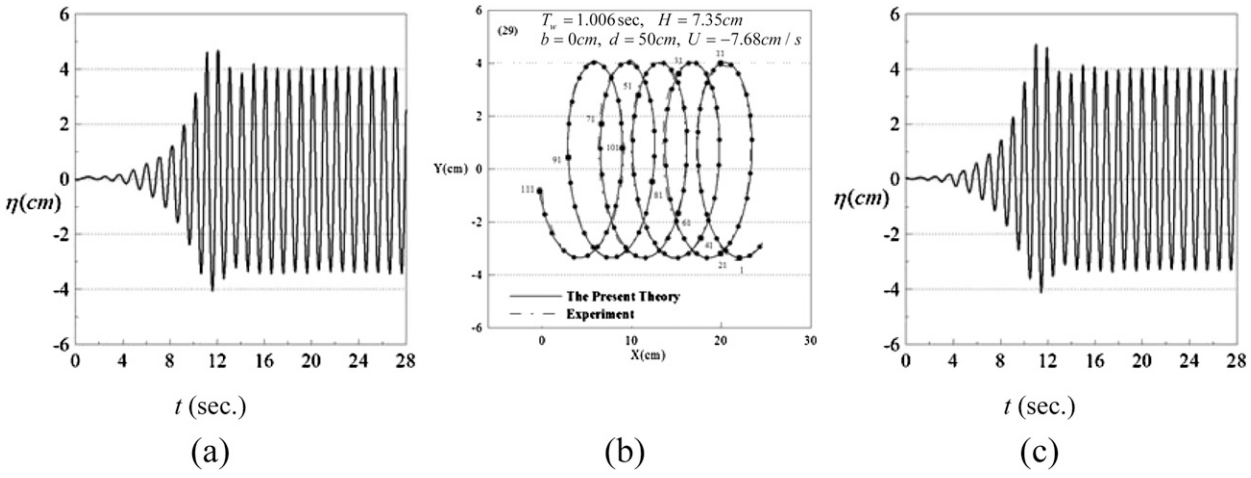

FIG. 7. As in Fig. 5, but for progressive waves with an adverse current.

stabilizing, the current variations are in general small, and the mean current speeds are nearly similar but are slower near the bottom, indicating that the generated current is satisfactorily uniform. Figures 4b and 4c show that, after a short time from the start, the waves measured at the wave gauges are in a periodic steady state with each individual wave being very similar. Considering the uniformity of the current and the scale of the grid network for analyzing the PS images, the generated current speeds ($U = |\overline{U}|\cos\theta$) are controlled within the range of ± 11 cm s^{-1}, where $\theta = 0$ or π and a plus sign (+) refers to the following current and a minus sign (−), the adverse current. The generated wave period T_w is in the range of 0.9–1.5 s and the generated wave height is below 13 cm.

The measured data are used to validate the fifth-order Lagrangian solution from Chen and Chen (2013, manuscript submitted to *Commun. Math. Phys.*). The comparisons are shown in Fig. 8 and Table 1. Obviously, the measured data of the particle trajectory, the particle motion period $T_L(b)$, the particle transport velocity $U_M(b)$, the Lagrangian mean level $\eta_L(b)$, etc. are in close agreement with the fifth-order Lagrangian solution. We note that (a, b, c) are the Lagrangian labels, and k is the wavenumber calculated from the fifth-order Lagrangian solution. As indicated in Figs. 8(1)–8(36) for the comparisons of the fifth-order theoretical Lagrangian solution and measured data of the particle PS trajectories, the ratio of the root-mean-square error (RMSE) between the theoretical values and the experiment values of the particle positions (x, y) to the maximum horizontal displacement of particle over one wave period l—that is, RMSE/l—is at a maximum 3.5% and most parts are less than 1%.

4. Validation of wave–current properties and discussion

a. The b line and velocity distribution

In the previous section, we obtain that the particle trajectories of the same label b (or Lagrangian vertical label, since $\overline{y} = b$) are all similar, which also validates the fifth-order Lagrangian solution.

For clarity, the b line is denoted as the line connecting the positions of the consecutive particles of the same label b at a fixed time. The b line oscillates like a wave motion and its wave shape can be obtained from the trajectory solution from Chen and Chen (2013, manuscript submitted to *Commun. Math. Phys.*). That is, for $z = 0$ with $\theta = 0$ or π, $U = |\overline{U}|\cos\theta$, and $\sigma = \sigma(b)$, $\sigma_w = kc_w = 2\pi/T_w$, the solution is

$$kx - (\sigma_w + kU)t = (ka - \sigma t) + \sum_{n=1}^{\infty} kf_n(ka - \sigma t, kb),$$

$$\sigma = \sigma(b) = \sigma_0 + \sum_{n=1}^{\infty} \sigma_n, \quad -d \le b \le 0. \tag{1a}$$

$$ky = kb + \sum_{n=1}^{\infty} k[g_n(ka - \sigma t, kb) + g_n'(kb)],$$

$$\sigma = \sigma(b) = \sigma_0 + \sum_{n=1}^{\infty} \sigma_n \quad \text{for} \quad -d \le b \le 0. \tag{1b}$$

Substituting $f_1 \sim f_5$, $g_1 \sim g_5$, $g_1' \sim g_5'$, and $\sigma_0 \sim \sigma_4$, σ_w from the fifth-order Lagrangian solution into Eqs. (1a) and (1b) with given U, also considering only one oscillation $0 \le ka - \sigma t \le 2\pi$ [equivalently, $0 \le a \le L$ for a fixed t or $0 \ge t \ge -T_L(b)$ for a fixed a], we could obtain the particle vertical position (level), ky, and the

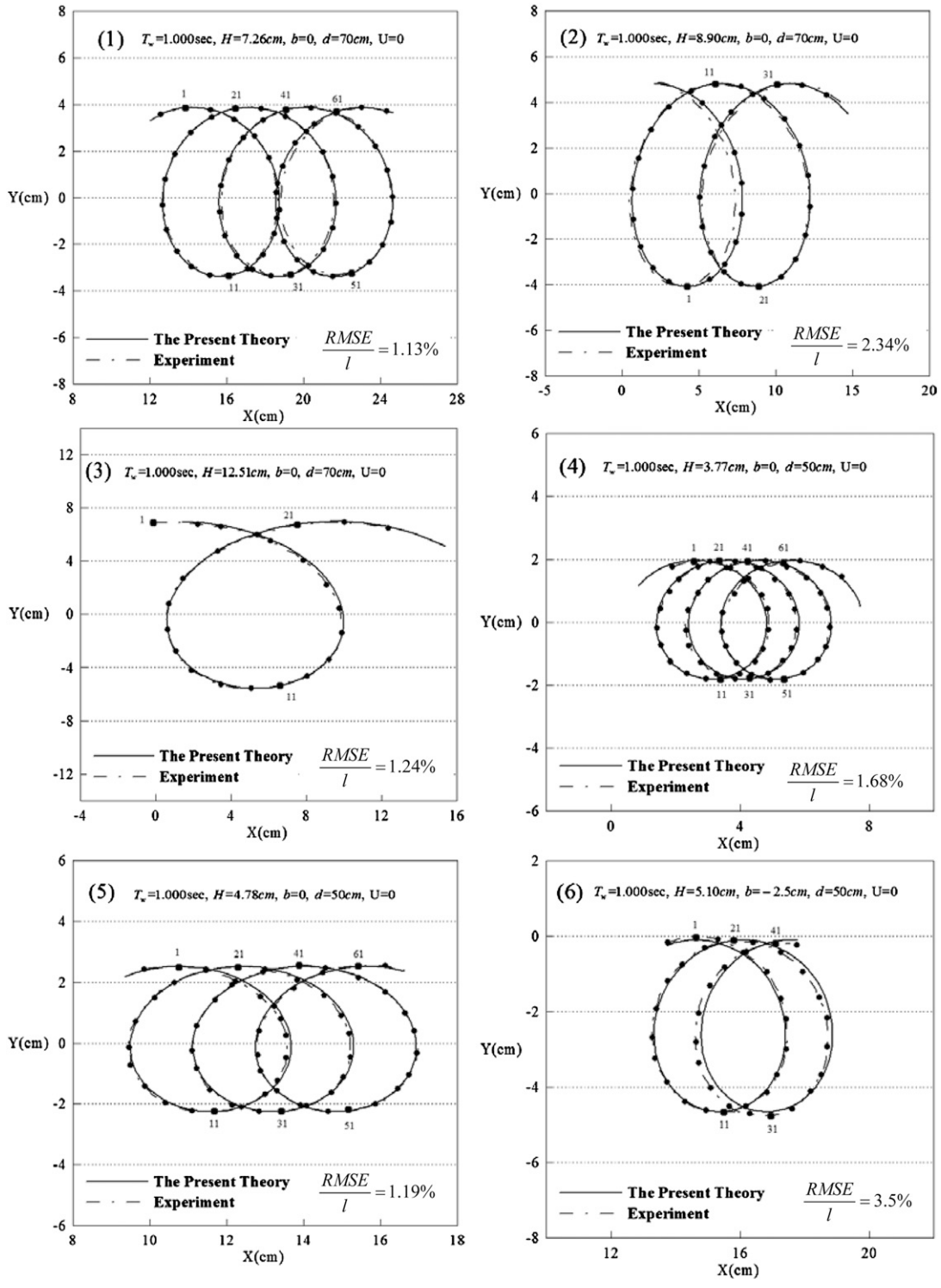

FIG. 8. Comparisons of trajectories between the measured data and the fifth-order Lagrangian solution. Dot 1 is the trajectory crest or trough, which occurs at the same vertical cross section as the wave crest or trough. The interval between two consecutive dots is $T_w/20$, T_w is the progressive wave period, U is the uniform current speed, H is the progressive wave height, d is the still water depth, b is the Lagrangian vertical label of the PS particle, and l is the maximum horizontal displacement of particle over one wave period.

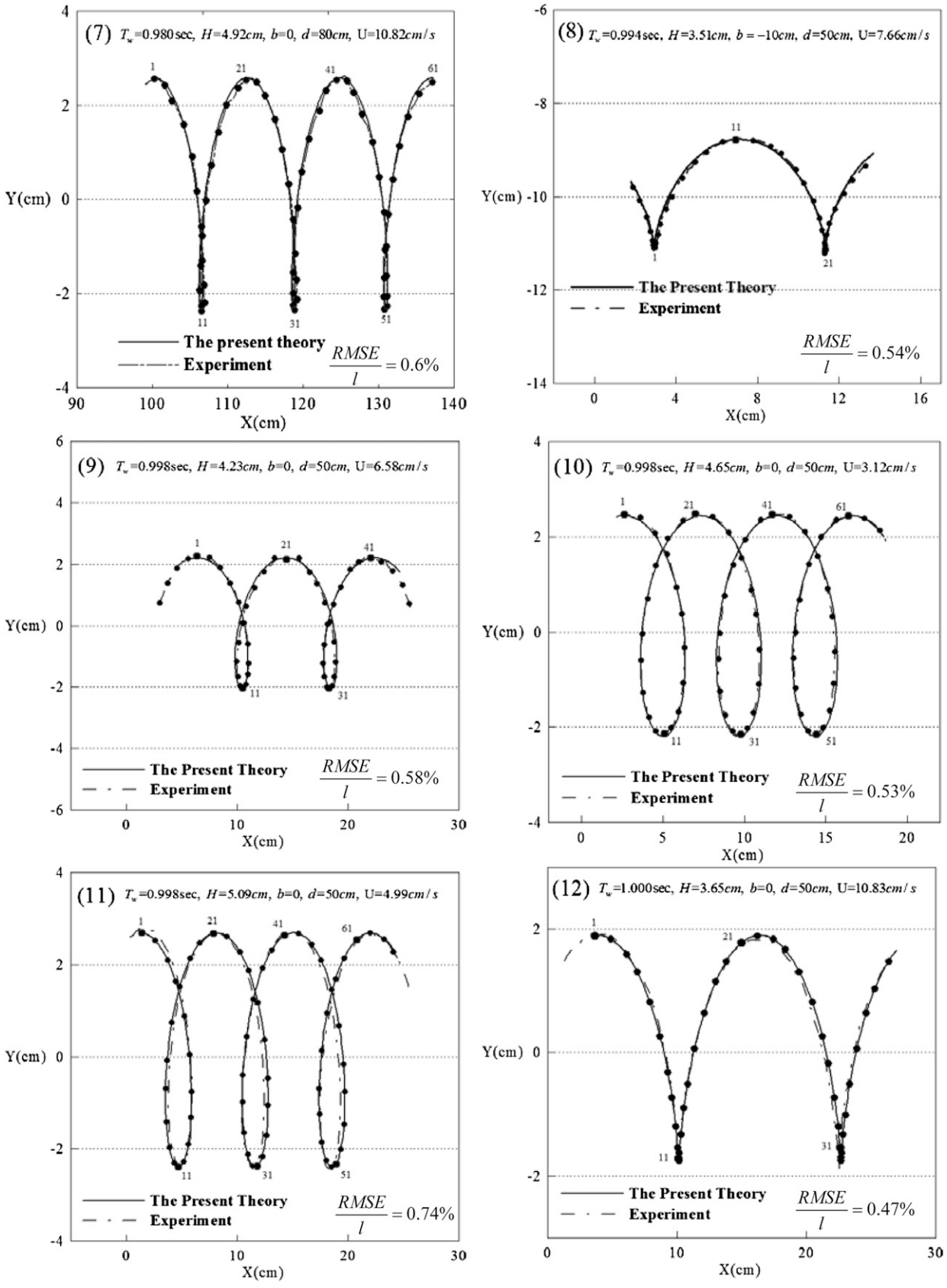

FIG. 8. (*Continued*)

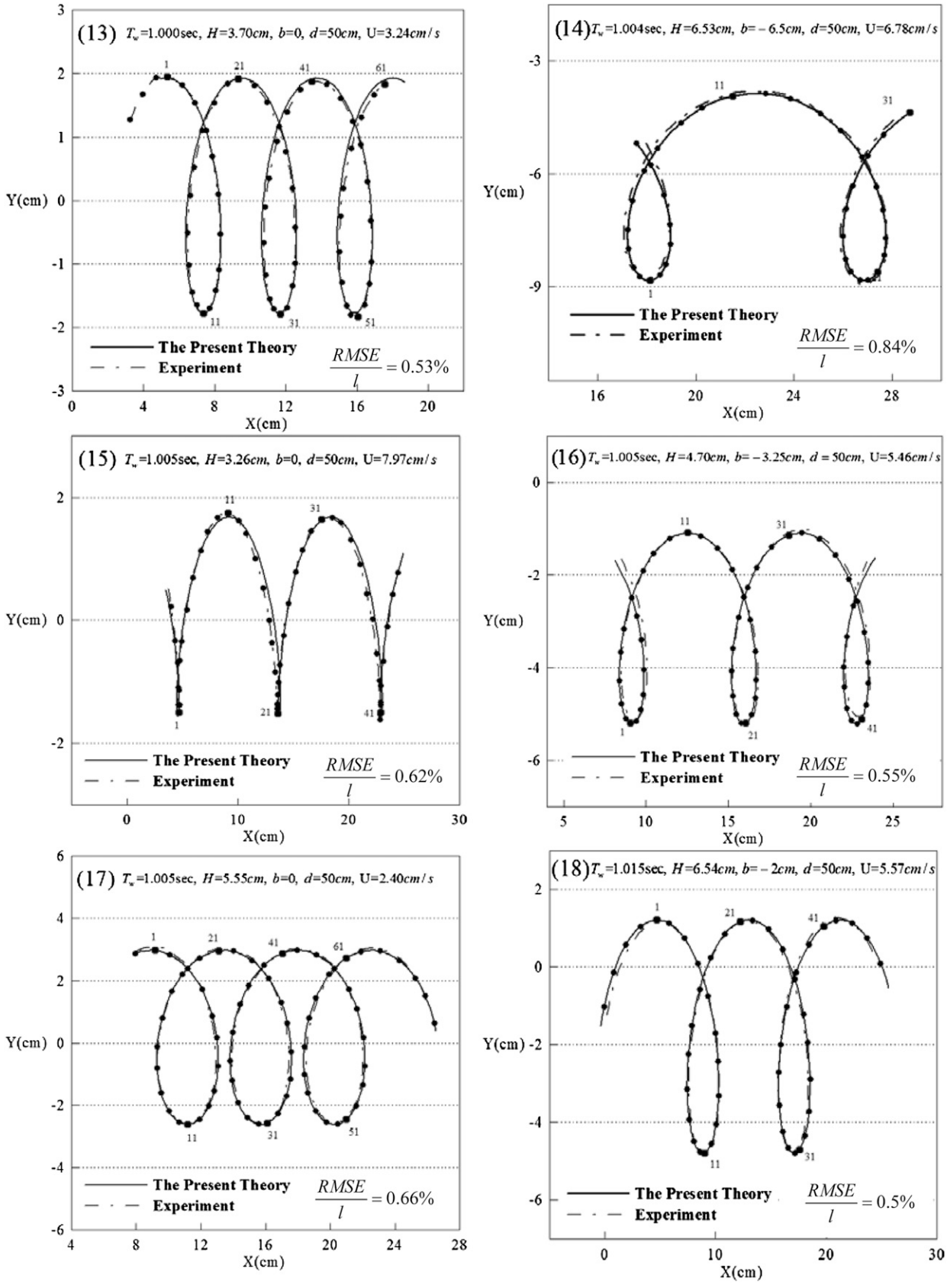

FIG. 8. (*Continued*)

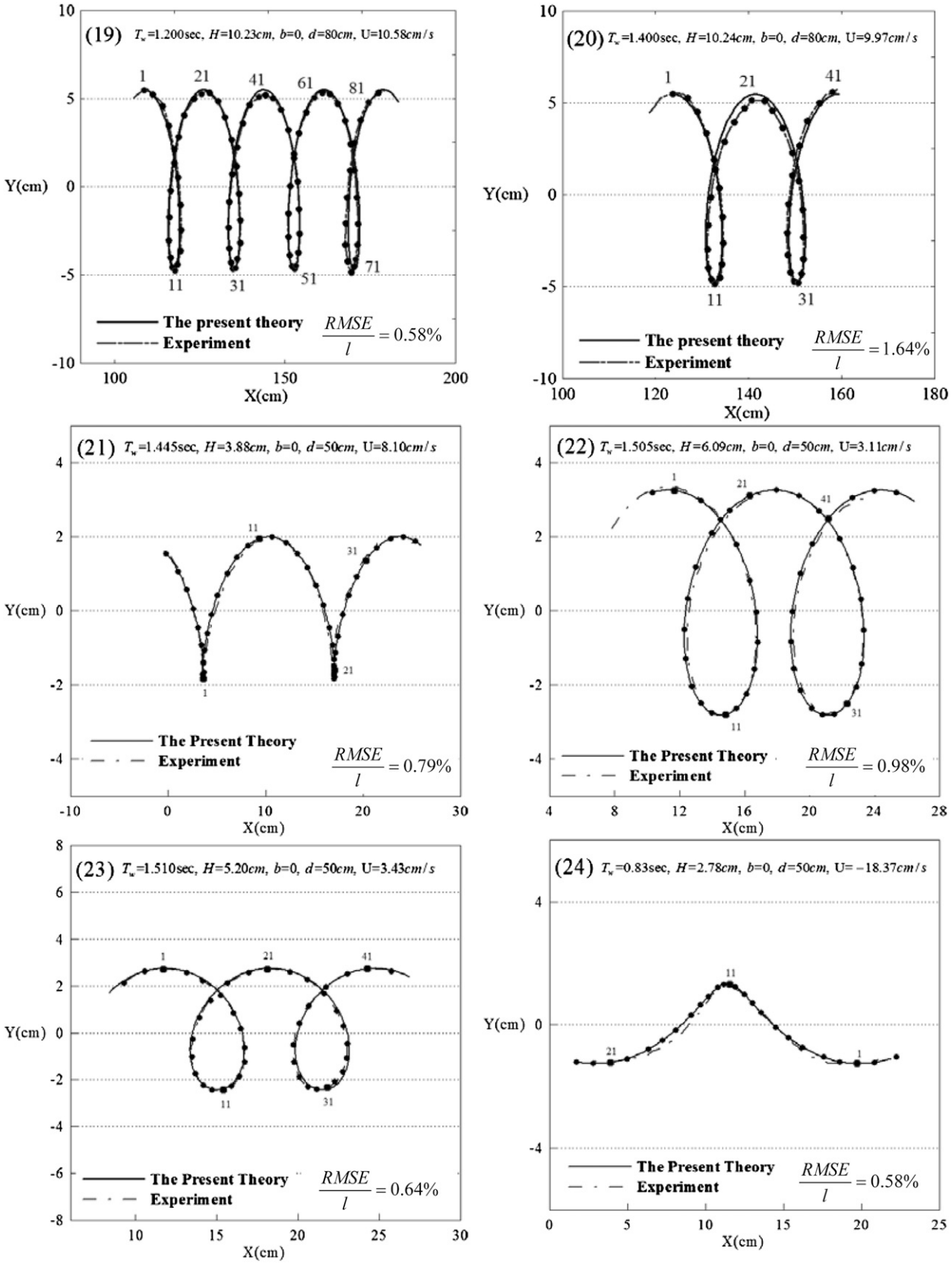

FIG. 8. (*Continued*)

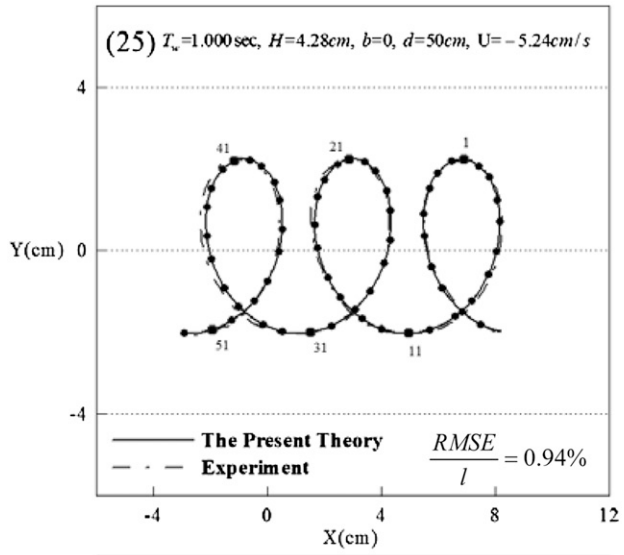

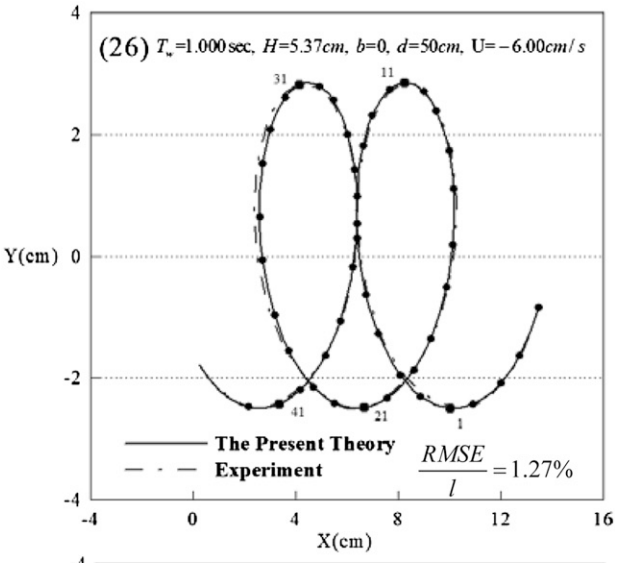

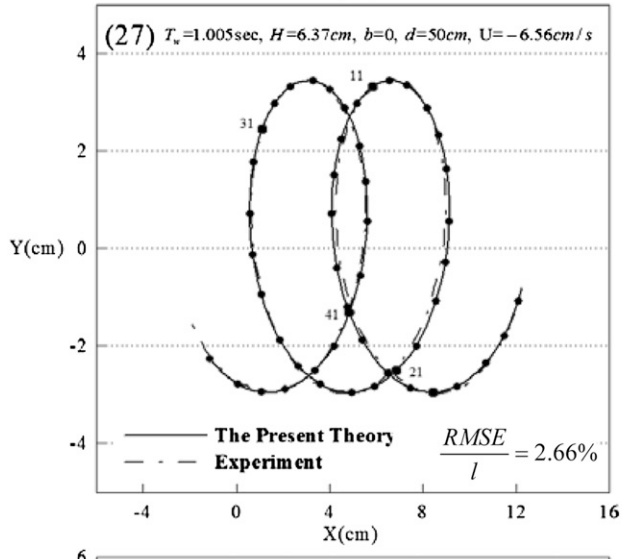

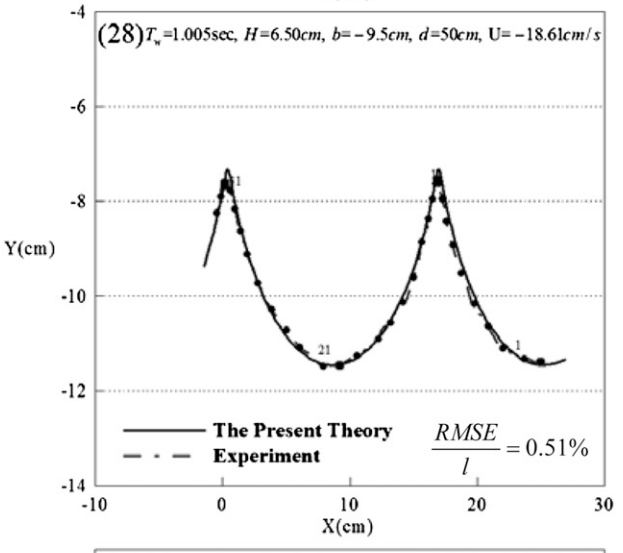

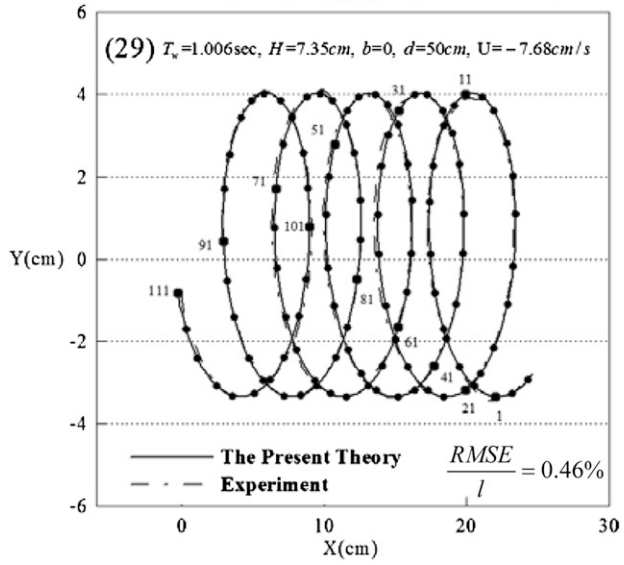

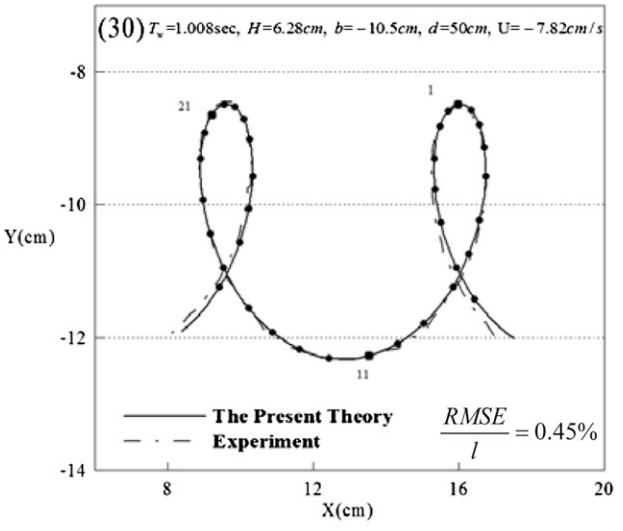

FIG. 8. (*Continued*)

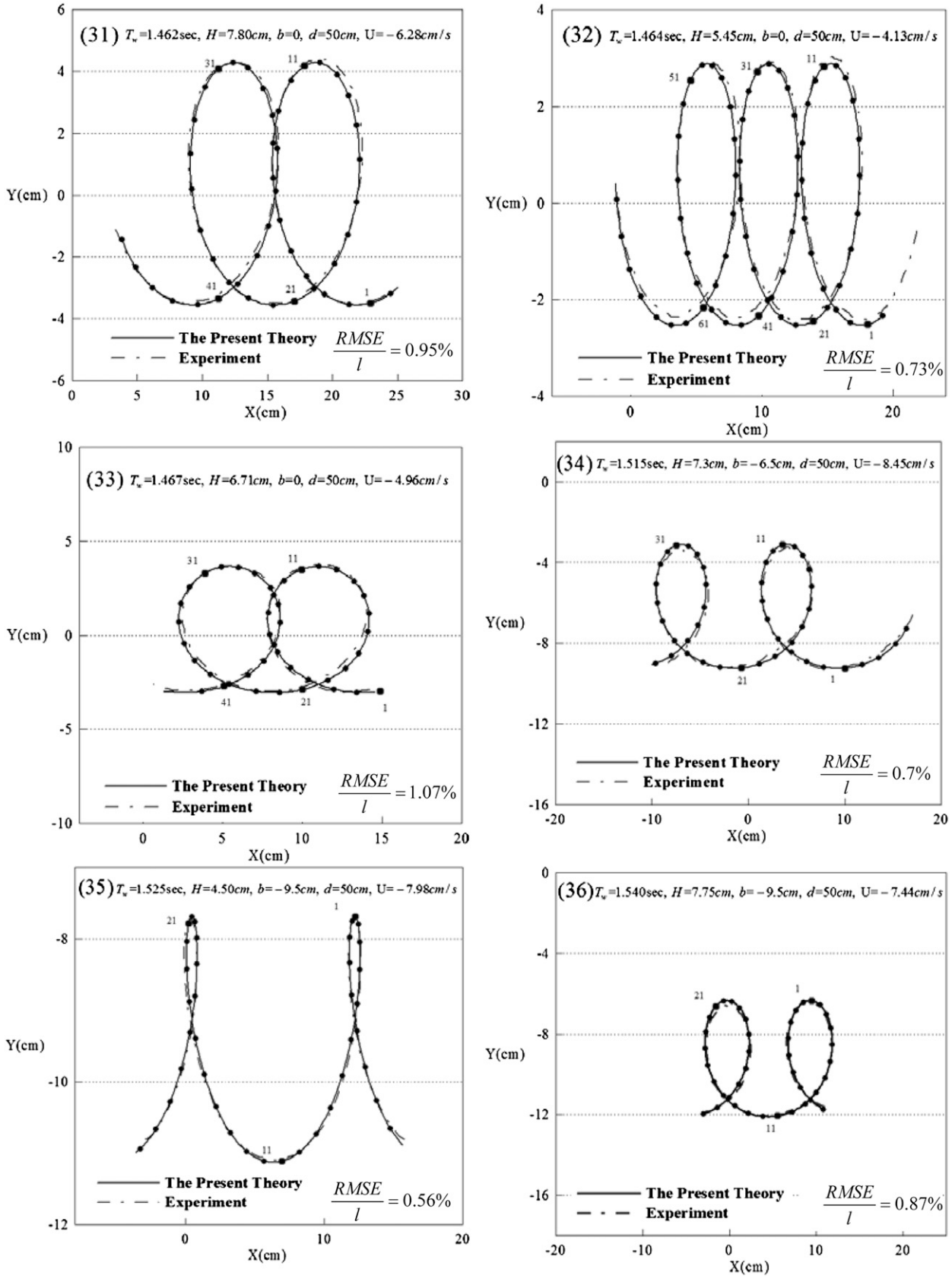

FIG. 8. (*Continued*)

TABLE 1. Comparisons of particle motion period $T_L(b)$, particle transport velocity $U_M(b)$, and Lagrangian mean level $\overline{\eta}_L(b)$ between the measured data and the fifth-order Lagrangian solution, where T_w is the wave period, d is the depth, and H is the wave height.

								$T_L(b)$ (s)		$[U_M(b) - U]$ (cm s^{-1})		$\overline{\eta}_L(b)$ (cm)	
No.	T_w (s)	d (cm)	H (cm)	b (cm)	H/L	d/L	U (cm s^{-1})	Measured	Theory	Measured	Theory	Measured	Theory
1	1.00	70	7.26	0.00	0.040	0.381	0.00	1.019	1.017	2.68	2.65	0.24	0.23
2	1.00	70	8.90	0.00	0.048	0.375	0.00	1.024	1.023	3.94	3.91	0.36	0.34
3	1.00	70	12.51	0.00	0.066	0.370	0.00	1.049	1.047	7.72	7.68	0.68	0.66
4	1.00	50	3.77	0.00	0.025	0.328	0.00	1.008	1.007	0.95	0.94	0.09	0.08
5	1.00	50	4.78	0.00	0.032	0.337	0.00	1.013	1.011	1.58	1.57	0.13	0.12
6	1.00	50	5.10	−2.50	0.034	0.333	0.00	1.014	1.011	1.44	1.42	0.15	0.14
7	0.98	80	4.92	0.00	0.033	0.529	10.82	0.993	0.990	1.64	1.62	0.14	0.13
8	0.99	50	3.51	−10.00	0.021	0.306	7.66	1.000	0.997	0.35	0.34	0.06	0.06
9	1.00	50	4.23	0.00	0.026	0.307	6.58	1.009	1.006	1.10	1.09	0.10	0.09
10	1.00	50	4.65	0.00	0.030	0.318	3.12	1.010	1.007	1.41	1.39	0.12	0.12
11	1.00	50	5.09	0.00	0.032	0.311	4.99	1.011	1.009	1.63	1.61	0.14	0.13
12	1.00	50	3.65	0.00	0.021	0.289	10.83	1.007	1.006	0.75	0.74	0.06	0.06
13	1.00	50	3.70	0.00	0.023	0.317	3.24	1.008	1.006	0.89	0.87	0.07	0.07
14	1.00	50	6.53	−6.50	0.039	0.301	6.78	1.017	1.015	1.55	1.53	0.22	0.21
15	1.01	50	3.26	0.00	0.020	0.300	7.97	1.012	1.010	0.63	0.62	0.05	0.05
16	1.01	50	4.70	−3.25	0.029	0.306	5.46	1.015	1.014	1.05	1.04	0.12	0.11
17	1.01	50	5.55	0.00	0.035	0.315	2.40	1.020	1.018	1.97	1.96	0.16	0.16
18	1.02	50	6.54	−2.00	0.039	0.299	5.57	1.032	1.030	2.17	2.16	0.22	0.21
19	1.20	80	10.23	0.00	0.046	0.356	10.58	1.230	1.226	3.95	3.93	0.39	0.37
20	1.40	80	10.24	0.00	0.035	0.275	9.97	1.422	1.410	2.76	2.72	0.33	0.30
21	1.45	50	3.88	0.00	0.014	0.175	8.10	1.452	1.451	0.45	0.44	0.06	0.05
22	1.51	50	6.09	0.00	0.022	0.179	3.11	1.521	1.519	1.14	1.12	0.14	0.13
23	1.51	50	5.20	0.00	0.019	0.179	3.43	1.517	1.515	0.83	0.82	0.10	0.09
24	0.83	50	2.78	0.00	0.021	0.371	−18.37	0.936	0.934	0.64	0.62	0.06	0.05
25	1.00	50	4.28	0.00	0.030	0.349	−5.24	1.012	1.010	1.36	1.34	0.11	0.10
26	1.00	50	5.37	0.00	0.038	0.351	−6.00	1.020	1.016	2.16	2.14	0.17	0.16
27	1.01	50	6.37	0.00	0.044	0.348	−6.56	1.028	1.026	2.96	2.98	0.24	0.23
28	1.01	50	6.50	−9.50	0.046	0.354	−18.61	1.016	1.014	1.34	1.33	0.25	0.24
29	1.01	50	7.35	0.00	0.052	0.351	−7.68	1.038	1.035	4.04	4.02	0.31	0.30
30	1.01	50	6.28	−10.50	0.044	0.353	−7.82	1.018	1.016	1.15	1.13	0.23	0.22
31	1.46	50	7.80	0.00	0.030	0.190	−6.28	1.480	1.478	2.01	1.99	0.23	0.22
32	1.46	50	5.45	0.00	0.020	0.188	−4.13	1.473	1.472	0.97	0.95	0.12	0.11
33	1.47	50	6.71	0.00	0.025	0.188	−4.96	1.482	1.480	1.47	1.45	0.17	0.16
34	1.52	50	7.73	−6.50	0.028	0.184	−8.45	1.529	1.527	1.40	1.40	0.21	0.21
35	1.53	50	4.50	−9.50	0.016	0.183	−7.98	1.536	1.532	0.41	0.39	0.07	0.07
36	1.54	50	7.75	−9.50	0.028	0.179	−8.21	1.553	1.552	1.21	1.20	0.21	0.21

horizontal position, $kx - (\sigma_w + kU)t$. The position of the b line is shown in Fig. 9. The particle velocity on the b line is calculated as follows: for the fixed labels (a, b) on the particle trajectory (x, y), the corresponding position (x, y) of the particle on the b line could be found from Eqs. (1a) and (1b) by matching the same phase $(ka - \sigma t)$ in $0 \geq t \geq -T_L(b)$. Once the particle position (x, y) is obtained, calculation of the velocity (x_t, y_t) is straightforward and the results are shown in Fig. 9. Figure 9 also shows the comparisons between the measured data and the fifth-order Lagrangian solution; their agreements are very good.

From the results, the motion of the b line behaves like a train of waves propagating in the x direction with the wave period $T = 2\pi/(\sigma_w + kU)$ and the propagating speed V being the sum of the progressive wave speed c_w and the current speed U, that is, $V = c_w + U$, depicting the Doppler effect. Obviously, these properties could be completely described by the fifth-order Lagrangian solution as illustrated in Fig. 9.

For depth variation of the particle velocity at wave crest $ka - \sigma t = 0$ and trough $ka - \sigma t = \pi$, we compare the measured data of Thomas (1981, 1990) with the fifth-order Lagrangian solution as shown in Fig. 10. They are in close agreement.

b. Particle trajectory for various uniform currents

Many theoretical particle trajectories for various uniform currents are already presented in section 4b of Chen and Chen (2013, manuscript submitted to

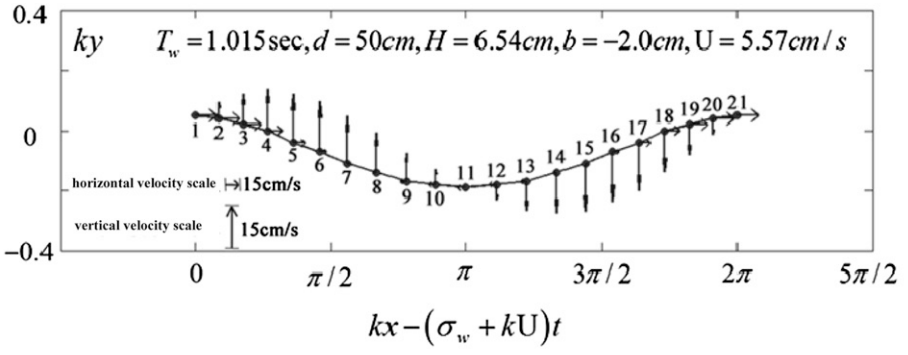

Point Number		1	2	3	4	5	6	7	8	9	10	11	12	13	14	15	16	17	18	19	20	21
$kx-(\sigma_w+kU)t$	*Exp.*	0.00	0.27	0.55	0.84	1.14	1.44	1.76	2.10	2.44	2.79	3.14	3.49	3.84	4.19	4.52	4.84	5.15	5.44	5.73	6.01	6.28
	The.	0.00	0.27	0.55	0.84	1.14	1.44	1.76	2.10	2.44	2.79	3.14	3.49	3.84	4.19	4.52	4.84	5.15	5.44	5.73	6.01	6.28
ky	*Exp.*	0.05	0.04	0.02	0.00	-0.04	-0.07	-0.11	-0.14	-0.17	-0.18	-0.19	-0.18	-0.17	-0.14	-0.11	-0.07	-0.04	0.00	0.02	0.04	0.05
	The.	0.05	0.04	0.02	0.00	-0.04	-0.07	-0.11	-0.14	-0.17	-0.18	-0.19	-0.18	-0.17	-0.14	-0.11	-0.07	-0.04	0.00	0.02	0.04	0.05
u(cm/s)	*Exp*	26.55	25.60	22.90	18.70	13.50	7.76	2.05	-3.03	-7.00	-9.55	-10.41	-9.54	-7.01	-3.04	2.08	7.76	13.50	18.72	22.90	25.60	26.54
	The.	26.51	25.58	22.88	18.69	13.48	7.74	2.04	-3.01	-6.98	-9.53	-10.39	-9.52	-6.99	-3.02	2.06	7.74	13.48	18.70	22.88	25.58	26.51
v(cm/s)	*Exp.*	0.00	5.79	11.00	15.02	17.51	18.25	17.20	14.52	10.48	5.51	0.00	-5.52	-10.46	-14.51	-17.20	-18.23	-17.52	-15.02	-11.00	-5.80	0.00
	The.	0.00	5.77	10.98	14.98	17.49	18.24	17.18	14.50	10.46	5.49	0.00	-5.49	-10.45	-14.49	-17.18	-18.22	-17.50	-14.98	-10.98	-5.79	0.00

(a)

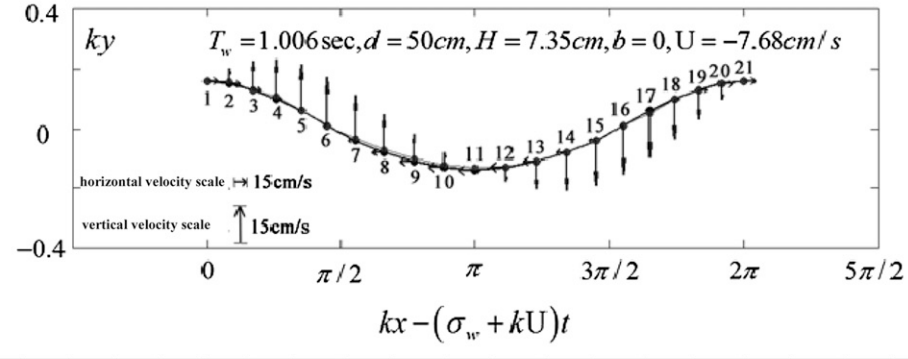

Point Number		1	2	3	4	5	6	7	8	9	10	11	12	13	14	15	16	17	18	19	20	21
$kx-(\sigma_w+kU)t$	*Exp.*	0.00	0.27	0.54	0.81	1.11	1.41	1.74	2.07	2.42	2.78	3.14	3.50	3.86	4.21	4.55	4.87	5.18	5.47	5.75	6.02	6.28
	The.	0.00	0.27	0.54	0.81	1.11	1.41	1.74	2.07	2.42	2.78	3.14	3.50	3.86	4.21	4.55	4.87	5.18	5.47	5.75	6.02	6.28
y	*Exp.*	0.16	0.16	0.13	0.11	0.06	0.01	-0.03	-0.07	-0.10	-0.12	-0.13	-0.13	-0.11	-0.08	-0.04	0.01	0.05	0.10	0.13	0.15	0.16
	The.	0.16	0.15	0.13	0.10	0.06	0.01	-0.04	-0.08	-0.11	-0.13	-0.14	-0.13	-0.11	-0.08	-0.04	0.01	0.06	0.10	0.13	0.15	0.16
u(cm/s)	*Exp*	17.63	16.54	13.35	8.43	2.28	-4.48	-11.14	-17.01	-21.63	-24.52	-25.55	-24.53	-21.61	-17.02	-11.13	-4.51	2.31	8.44	13.40	16.55	17.65
	The.	17.61	16.51	13.33	8.41	2.27	-4.46	-11.11	-16.97	-21.60	-24.50	-25.52	-24.51	-21.59	-16.99	-11.11	-4.48	2.29	8.42	13.37	16.53	17.63
v(cm/s)	*Exp.*	0.00	7.20	13.60	18.58	21.65	22.54	21.20	17.84	12.85	6.73	0.00	-6.72	-12.86	-17.85	-21.21	-22.53	-21.64	-18.57	-13.60	-7.20	0.00
	The.	0.00	7.17	13.56	18.55	21.62	22.51	21.18	17.82	12.83	6.71	0.00	-6.70	-12.83	-17.83	-21.19	-22.51	-21.62	-18.55	-13.57	-7.18	0.00

(b)

FIG. 9. Wave shape of the *b* line and particle velocity on the *b* line from the measured data and the fifth-order Lagrangian solution (a) under free surface and (b) on free surface.

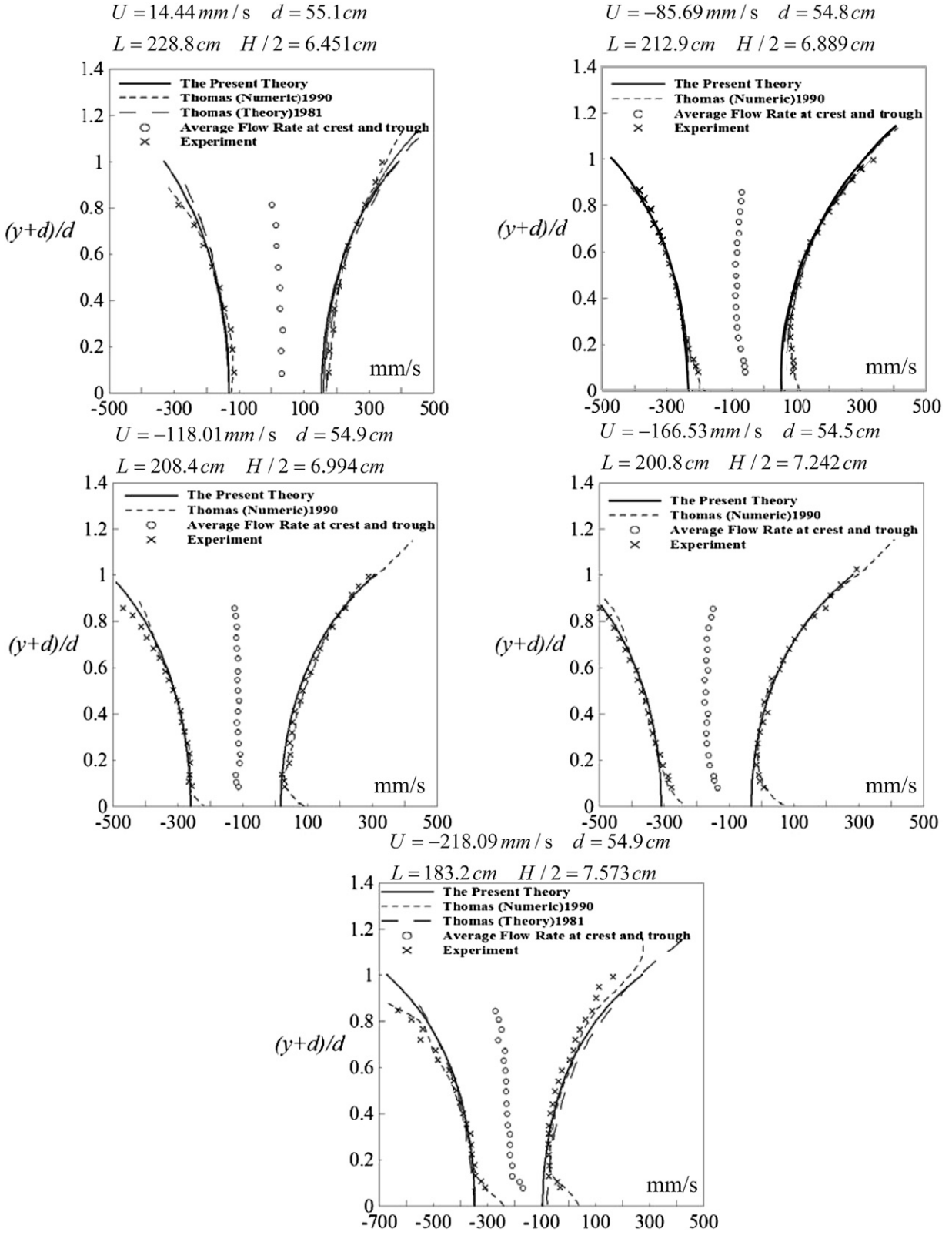

FIG. 10. Comparison of particle velocities through depth at the wave crest and trough between the measured data by Thomas (1981, 1990) and the fifth-order Lagrangian solution.

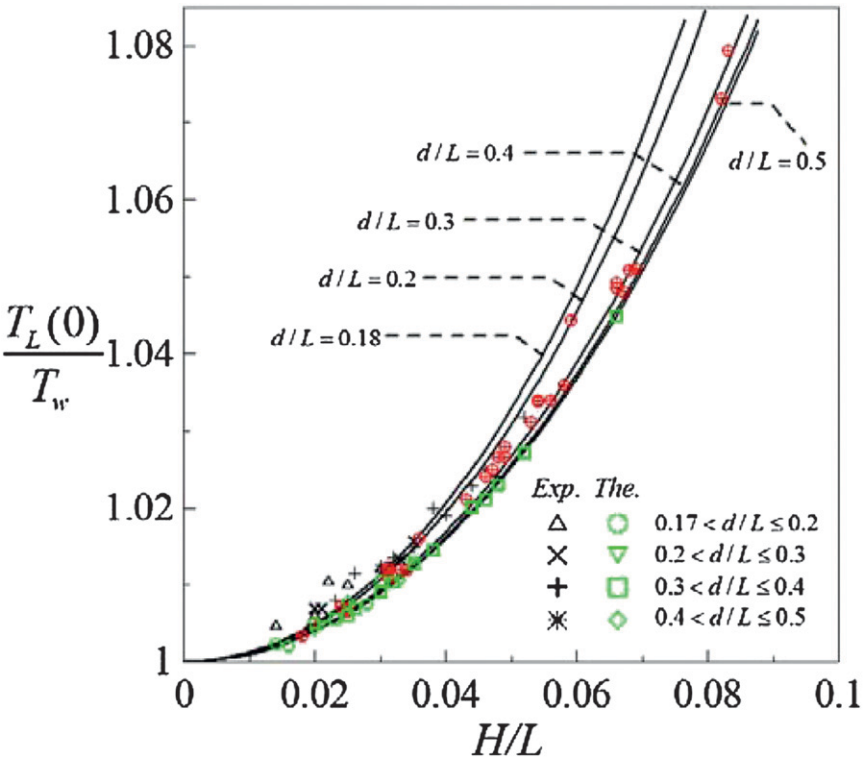

FIG. 11. Particle motion period at the free surface $T_L(0)/T_w$ vs wave steepness H/L and relative water depth d/L for the measured data and the fifth-order Lagrangian solution: T_w is the progressive wave period and $\oplus$ is the measured data from the experiment by Chen et al. (2010).

Commun. Math. Phys.). In this section, the trajectories from the fifth-order Lagrangian solution are validated by the measured data for following, no, and adverse currents.

1) FOLLOWING CURRENT, $U = |\overline{U}| \cos 0^o > 0$

Corresponding to Eqs. (99a)–(99c) in Chen and Chen (2013, manuscript submitted to *Commun. Math. Phys.*) there are three different conditions for shaping the trajectory as follows:

(i) When

$$x_t = U + \sum_{n=1}^{5} \{f_{nt}[ka - \sigma t = (2j+1)\pi,\ kb] + f'_{nt}(kb, \sigma_0 t)\} < 0, \quad j \in I, \quad -d \le b \le 0, \tag{2a}$$

where I denotes integer. The motion of the (a, b) particle is a two-dimensional (2D) periodic trajectory, which is like the prolate trochoid and moves in the following direction as shown in Figs. 8(9)–8(11), 8(13), 8(14), 8(16)–8(20), 8(22), and 8(23).

(ii) When

$$x_t = U + \sum_{n=1}^{5} \{f_{nt}[ka - \sigma t = (2j+1)\pi, kb] + f'_{nt}(kb, \sigma_0 t)\} = 0, \quad j \in I, \quad -d \le b \le 0. \tag{2b}$$

The motion of the (a, b) particle is also a 2D periodic trajectory, which is like the cycloid with sharp-point troughs and moves in the following direction as shown in Figs. 8(7), 8(8), and 8(15).

(iii) When

$$x_t = U + \sum_{n=1}^{5} \{f_{nt}[ka - \sigma t = (2j+1)\pi, kb] + f'_{nt}(kb, \sigma_0 t)\} > 0, \quad j \in I, \quad -d \le b \le 0. \tag{2c}$$

The motion of the (a, b) particle is also a 2D periodic trajectory which is like the curtate trochoid and moves in the following direction as shown in Figs. 8(12) and 8(21).

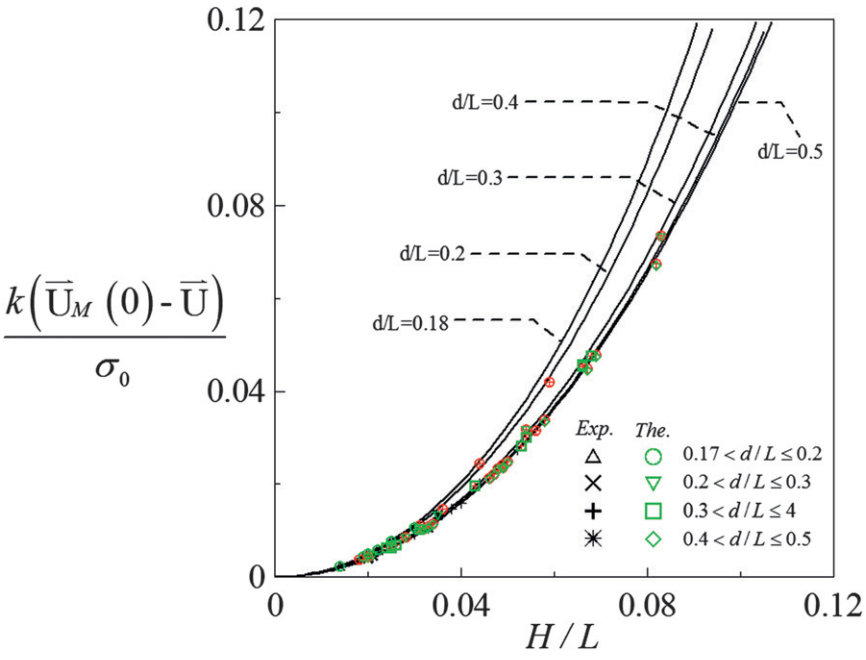

FIG. 12. Particle transport velocity at the free surface less the current $k[U_M(0) - U]/\sigma_0$ vs wave steepness H/L and relative water depth d/L for the measured data and the fifth-order Lagrangian solution: ⊕ is the measured data from the experiment by Chen et al. (2010).

From the figures mentioned above, the fifth-order Lagrangian solution agrees closely with the measured data; Eqs. (2a)–(2c) are validated. From Eqs. (2a) to (2c), the shape of the trajectory is dominated by the horizontal particle velocity at the trajectory trough, $x_t[ka - \sigma t = (2j + 1)\pi, kb, \sigma_0 t]$, $j \in I$.

2) NO CURRENT, $U = |\overline{U}| = 0$

The motion of the (a, b) particle is a 2D periodic trajectory, which is like the prolate trochoid, and moves in the following direction as shown in Figs. 8(1)–8(6), similar to Fig. 4 of Chen et al. (2010). The comparisons in the figure obviously show close agreement between the measured data and the fifth-order Lagrangian solution.

3) ADVERSE CURRENT, $U = |\overline{U}|\cos\pi < 0$

Corresponding to Eqs. (100a)–(100e) in Chen and Chen (2013, manuscript submitted to *Commun. Math. Phys.*), there are five different conditions for the shaping trajectory as follows:

(i) When

$$U + \sum_{n=1}^{5} f'_{nt}(kb, \sigma_0 t) > 0, \quad -d \le b \le 0. \tag{3a}$$

The motion of the (a, b) particle is a 2D periodic trajectory, which is like the prolate trochoid with a shorter horizontal axis and moves in the following direction.

(ii) When

$$U + \sum_{n=1}^{5} f'_{nt}(kb, \sigma_0 t) = 0, \quad -d \le b \le 0. \tag{3b}$$

The motion of the (a, b) particle is a 2D periodic trajectory, which is like an elliptic curve with a longer horizontal axis.

(iii) When

$$U + \sum_{n=1}^{5} f'_{nt}(kb, \sigma_0 t) < 0 < x_t$$

$$= U + \sum_{n=1}^{5} [f_{nt}(ka - \sigma t = 2j\pi, kb) + f'_{nt}(kb, \sigma_0 t)]$$

$$j \in I, \quad -d \le b \le 0. \tag{3c}$$

The motion of the (a, b) particle is a 2D periodic trajectory, which is like the turned prolate trochoid and moves in the adverse direction as shown in Figs. 8(25)–8(27) and 8(29)–8(36).

(iv) When

$$x_t = U + \sum_{n=1}^{5} [f_{nt}(ka - \sigma t = 2j\pi, kb) + f'_{nt}(kb, \sigma_0 t)] = 0,$$

$$j \in I, \quad -d \le b \le 0. \tag{3d}$$

The motion of the (a, b) particle is a 2D periodic trajectory, which is like the turned cycloid with the

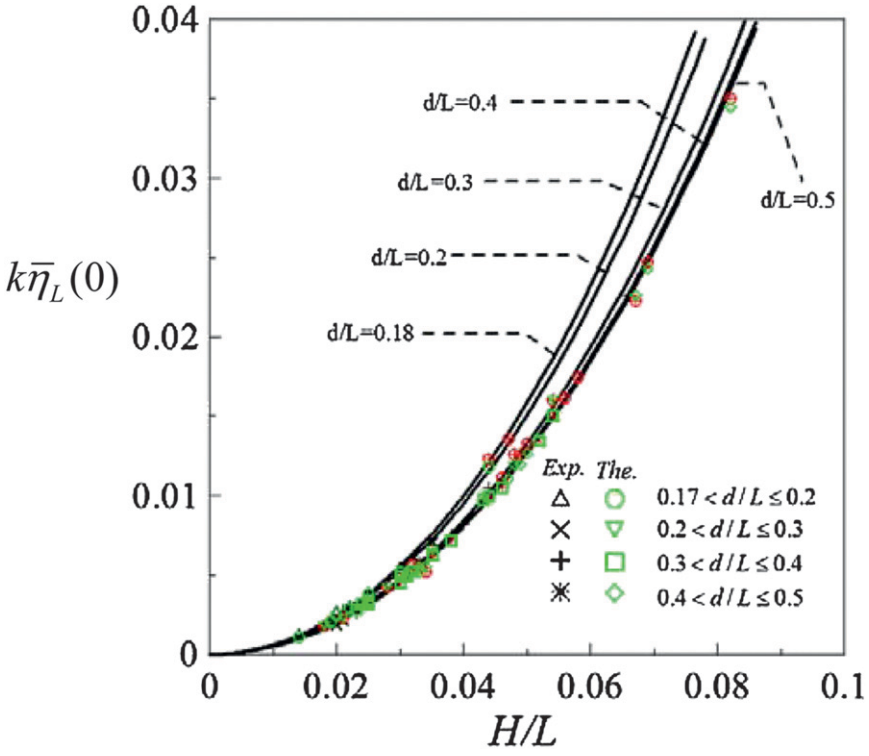

FIG. 13. Lagrangian mean level at free surface $k\overline{\eta}_L(0)$ vs wave steepness H/L and relative water depth d/L for the measured data and the fifth-order Lagrangian solution: ⊕ is the measured data from the experiment by Chen et al. (2010).

sharp-point crests and moves in the adverse direction as shown in Fig. 8(28).

(v) When

$$x_t = U + \sum_{n=1}^{5} [f_{nt}(ka - \sigma t = 2j\pi, kb) + f'_{nt}(kb, \sigma_0 t)] < 0,$$
$$j \in I, \quad -d \le b \le 0. \tag{3e}$$

The motion of the (a, b) particle is a 2D periodic trajectory, which is like the turned curtate trochoid and moves in the adverse direction as shown in Fig. 8(24).

The figures mentioned above show that the fifth-order Lagrangian solution agrees closely with the measured data, and Eqs. (3a)–(3e) are thus validated. Obviously, from Eqs. (3a) to (3e), the shape of the trajectory is dominated by the horizontal particle transport velocity at trajectory crests, and its drift velocity is $U + \sum_{n=1}^{5} f'_{nt}(kb, \sigma_0 t)$.

c. Particle motion period $T_L(b)$ and frequency $\sigma(b) = 2\pi/T_L(b)$

The particle motion period $T_L(b)$ and frequency $\sigma(b) = 2\pi/T_L(b)$ for the fifth-order Lagrangian solution are given by Eq. (95) in Chen and Chen (2013, manuscript submitted to *Commun. Math. Phys.*),

$$\sigma(b) = 2\pi/T_L(b) = 2\pi/T_w - k[f'_{2t}(kb, \sigma_0 t) + f'_{4t}(kb, \sigma_0 t)] = \sigma_0 + \sigma_2(b) + \sigma_4(b). \tag{4}$$

Comparisons of $T_L(b)$ calculated from Eq. (4) and from the measured data are shown in Table 1 and Fig. 11. Note that Fig. 11 shows the particle motion period only at the free surface, $b = 0$. The comparisons agree well. From this result and Fig. 9, it indicates that the wave period of the line is affected by the current, that is, by the Doppler effect. However, the particle motion period is not affected by the current; it has the same wave period of the progressive waves in the absence of current. These motion properties are the same as described in section 4.2 in Chen and Chen (2013, manuscript submitted to *Commun. Math. Phys.*).

d. Particle transport velocity (drift velocity) $U_M(b)$

The particle transport velocity, so-called drift velocity, is described by Eq. (96) in Chen and Chen (2013, manuscript submitted to *Commun. Math. Phys.*),

$$U_M(b) = U + f'_{2t}(kb, \sigma_0 t) + f'_{4t}(kb, \sigma_0 t) = U + [2\pi/T_w - 2\pi/T_L(b)]/k. \quad (5)$$

From Eq. (5), $U_M - U$ is a relative velocity identical to the case of progressive waves in the absence of current. The property of $U_M - U$ is already described in section 4.2 in Chen and Chen (2013, manuscript submitted to *Commun. Math. Phys.*). Comparisons of the measured data and the fifth-order Lagrangian solution are shown in Table 1 and Fig. 12. Note that Fig. 12 shows only the case at the free surface, $b = 0$. The comparisons show close agreement.

e. Period-mean level of particle motion or particle Lagrangian mean level $\overline{\eta}_L(b)$

The Lagrangian mean level is described by Eq. (97) in Chen and Chen (2013, manuscript submitted to *Commun. Math. Phys.*),

$$\overline{\eta}_L(b) = \frac{1}{T_L(b)} \int_0^{T_L(b)} (y - b)\, dt = g'_2(kb) + g'_4(kb) \geq 0. \quad (6)$$

Equation (6) indicates the Lagrangian mean level is not affected by the current. Its property is already described in section 4.2 in Chen and Chen (2013, manuscript submitted to *Commun. Math. Phys.*). Comparisons of the measured data and the fifth-order Lagrangian solution are shown in Table 1 and Fig. 13. Note that Fig. 13 shows only the case at the free surface, $b = 0$. The comparisons show close agreement.

5. Conclusions

In Chen and Chen (2013, manuscript submitted to *Commun. Math. Phys.*), the fifth-order Lagrangian solution for the irrotational, free-surface periodic water waves propagating on uniform current is presented. In this experimental investigation, the following, no, and adverse currents are considered. The measured data of the *b* line, the particle velocity, the particle trajectory, the particle motion period, the particle transport velocity, the Lagrangian mean level, etc., are all in close agreement with the fifth-order Lagrangian solution. Below are several interesting points.

Lagrangian label (a, b) of a particle in wave motion could adopt the coordinates of the particle position in the still water.

The *b* line could be described by the trajectory of a particle in Eqs. (1a) and (1b). The wavelength of the *b* line is equal to the progressive wavelength, and the wave velocity of the *b* line is the sum of the progressive wave velocity and the current velocity, the Doppler effect. However, the particle motion period, the Lagrangian mean level, and the particle transport velocity less the current velocity are independent of the current and are equal to those of the progressive wave in the absence of current. These properties are described in section 4.2 in Chen and Chen (2013, manuscript submitted to *Commun. Math. Phys.*)

The particle trajectory in the following current is dominated by the horizontal particle velocity x_t at the trajectory trough. When $x_t < 0$ (in the adverse direction), the trajectory is like the prolate trochoids; when $x_t = 0$, the trajectory is like the cycloid with sharp-point troughs; when $x_t > 0$ (in the following direction), the trajectory is like the curtate trochoid. These trajectories all move in the following direction.

When in the case of the adverse current, the trajectory is dominated by the particle transport velocity U_M and the particle velocity x_t at the trajectory crest. When $U_M > 0$, the trajectory moves in the following direction and is like the prolate trochoid with a shorter horizontal axis; when $U_M = 0$, the trajectory is like an elliptic curve with a longer horizontal axis; when $U_M < 0$ and $x_t > 0$ at the trajectory crest, the trajectory moves in the adverse direction, and is like the turned prolate trochoid; when $U_M < 0$ and $x_t = 0$ at the trajectory crest, the trajectory moves in the adverse direction, and is like the turned cycloid with sharp-point crests; and when $U_M < 0$ and $x_t < 0$ at the trajectory crest, the trajectory moves in the adverse direction, and is like the turned curtate trochoid.

Finally, the fifth-order Lagrangian solution is obtained from the boundary value problem formulated and solved completely in the Lagrangian framework. The solution is shown to closely agree with the measured data. For a description of the flow motion, the Lagrangian solution could be more effective and precise than the Eulerian solution.

Acknowledgments. The support under Grant NSC 101-2622-E-006-010-CC2 from the National Science Council, Taiwan, is gratefully acknowledged.

REFERENCES

Baddour, R. E., and S. W. Song, 1990: Interaction of higher-order waves with uniform currents. *Ocean Eng.,* **17,** 551–568.

Chen, Y. Y., S. S. Lin, and L. S. Her, 1998: The Lagrangian properties of progressive gravity waves by experiment (in Chinese). *Proc. 20th Ocean Engineering Conf.,* Keelung, Taiwan, National Taiwan Ocean University, 60–70.

——, H.-C. Hsu, and G.-Y. Chen, 2010: Lagrangian experiment and solution for irrotational finite-amplitude progressive gravity waves at uniform depth. *Fluid Dyn. Res.,* **42,** 045511, doi:10.1088/0169-5983/42/4/045511.

——, ——, and H. H. Hwung, 2012: Particle trajectories beneath wave-current interaction in a two-dimensional field. *Nonlinear Processes Geophys.,* **19,** 185–197.

Davies, A. G., and A. D. Heathershaw, 1984: Surface-wave propagation over sinusoidally varying topography. *J. Fluid Mech.,* **144,** 419–443.

Groeneweg, J., and J. Battjes, 2003: Three dimensional wave effects on a steady current. *J. Fluid Mech.,* **478,** 325–343.

Jonsson, I. G., 1977: Energy flux and wave action in gravity waves propagating on a current. *J. Hydraul. Res.,* **16,** 223–234.

——, C. Skougaard, and J. D. Wang, 1970: Interaction between waves and currents. *Proc. 12th Conf. on Coastal Engineering,* Washington, D.C., ASCE, 489–507.

——, O. Brink-Kjaer, and G. P. Thomas, 1978: Wave motion and set-down for waves on a shear current. *J. Fluid Mech.,* **87,** 401–416.

Longuet-Higgins, M. S., 1986: Eulerian and Lagrangian aspects of surface waves. *J. Fluid Mech.,* **173,** 683–707.

——, and R. W. Stewart, 1960: Changes in the form of short gravity waves on long waves and tidal currents. *J. Fluid Mech.,* **8,** 565–583.

——, and ——, 1961: The changes in amplitude of short gravity waves on steady non-uniform current. *J. Fluid Mech.,* **10,** 529–549.

Morison, J. R., and R. C. Crooke, 1953: The mechanics of deep water, shallow water, and breaking wave. Corps of Engineers Beach Erosion Board Tech. Memo. 40, 22 pp.

Musumeci, R. E., L. Cavallo, E. Foti, P. Scandura, and P. Blondeaux, 2006: Waves plus currents crossing at a right angle: Experimental investigation. *J. Geophys. Res.,* **111,** C07019, doi:10.1029/2005JC002933.

Olabarrieta, M., P. Medina, and S. Castanedo, 2010: Effects of wave–current interaction on the current profile. *Coastal Eng.,* **57,** 643–665.

Peregrine, D. H., 1976: Interaction of water waves and currents. *Adv. Appl. Mech.,* **16,** 9–117.

Pullen, J., A. Arnott, J. M. Buick, and C. Greated, 1998: Lagrangian motions near the surface of capillary–gravity waves with surface active films. *Proc. EUROMECH 387,* Warwick, United Kingdom, European Mechanics Society 7 pp. [Available online at http://www.buickj.myweb.port.ac.uk/Publications/PDF/054m.PDF.]

Thomas, G. P., 1981: Wave-current interactions: An experimental and numerical study. Part 1. Linear waves. *J. Fluid Mech.,* **110,** 457–474.

——, 1990: Wave-current interactions: An experimental and numerical study. Part 2. Nonlinear waves. *J. Fluid Mech.,* **216,** 505–536.